



Towards radiocarbon calibration beyond 28 ka using speleothems from the Bahamas

Dirk L. Hoffmann^{a,b,*}, J. Warren Beck^c, David A. Richards^{a,b}, Peter L. Smart^b, Joy S. Singarayer^b, Tricia Ketchmark^c, Chris J. Hawkesworth^{a,d}

^a Bristol Isotope Group, University of Bristol, UK

^b School of Geographical Sciences, University of Bristol, University Road, BS8 1SS, Bristol, UK

^c NSF-Arizona AMS Facility, University of Arizona, Tucson, AZ 85721, USA

^d Department of Earth Sciences, University of Bristol, Queen's Road, BS8 1RJ, Bristol, UK

ARTICLE INFO

Article history:

Received 3 May 2009

Received in revised form 27 August 2009

Accepted 7 October 2009

Available online 26 November 2009

Editor: P. DeMenocal

Keywords:

radiocarbon
U–Th dating
speleothems
MIS 3
geomagnetic intensity
earth system models

ABSTRACT

We present a new speleothem record of atmospheric $\Delta^{14}\text{C}$ between 28 and 44 ka that offers considerable promise for resolving some of the uncertainty associated with existing radiocarbon calibration curves for this time period. The record is based on a comprehensive suite of AMS ^{14}C ages, using new low-blank protocols, and U–Th ages using high precision MC-ICPMS procedures. Atmospheric $\Delta^{14}\text{C}$ was calculated by correcting ^{14}C ages with a constant dead carbon fraction (DCF) of $22.7 \pm 5.9\%$, based on a comparison of stalagmite ^{14}C ages with the IntCal04 (Reimer et al., 2004) calibration curve between 15 and 11 ka. The new $\Delta^{14}\text{C}$ speleothem record shows similar structure and amplitude to that derived from Cariaco Basin foraminifera (Hughen et al., 2004, 2006), and the match is further improved if the latter is tied to the most recent Greenland ice core chronology (Svensson et al., 2008). These data are however in conflict with a previously published ^{14}C data set for a stalagmite record from the Bahamas – GB-89-24-1 (Beck et al., 2001), which likely suffered from ^{14}C analytical blank subtraction issues in the older part of the record. The new Bahamas speleothem $\Delta^{14}\text{C}$ data do not show the extreme shifts between 44 and 40 ka reported in the previous study (Beck et al., 2001). Causes for the observed structure in derived atmospheric $\Delta^{14}\text{C}$ variation based on the new speleothem data are investigated with a suite of simulations using an earth system model of intermediate complexity. Data-model comparison indicates that major fluctuations in atmospheric $\Delta^{14}\text{C}$ during marine isotope stage 3 is primarily a function of changes in geomagnetic field intensity, although ocean–atmosphere system reorganisation also played a supporting role.

© 2009 Elsevier B.V. All rights reserved.

1. Introduction

Accurate records of past atmospheric radiocarbon concentration ($\Delta^{14}\text{C}$) are essential for the calibration of the widely-used radiocarbon timescale (Reimer et al., 2004; Stuiver, 1982). Accurate records are also necessary in order to validate models of ^{14}C production rates in the upper atmosphere (Lal and Peters, 1967; Masarik and Beer, 1999), to constrain the flux of carbon transfer between earth system reservoirs (Broecker, 1963; Stuiver and Braziunas, 1993; Toggweiler et al., 1989) and to use ^{14}C as tracer for changes in past ocean circulation (Sarnthein et al., 2007). For the Holocene period, continuous tree-ring records are generally thought to provide reliable archives of past atmospheric $\Delta^{14}\text{C}$ variations (Stuiver, 1982). Major international efforts over the past 60 years have yielded continuous records from present day to 12.41 ka

BP (Friedrich et al., 2004), but only sparse, floating tree-ring records are found for time periods earlier than this. This has made it necessary to draw upon archives from the marine realm such as corals (Bard et al., 1990; Burr et al., 1992, 2004; Cutler et al., 2004; Fairbanks et al., 2005) and foraminifera (Bard et al., 2004c; Hughen et al., 2006, 1998) to infer $\Delta^{14}\text{C}$ and provide a calibration curve to 26 ka cal BP (Reimer et al., 2004). However, for times earlier than 26 ka cal BP no consensus has yet been achieved because of substantial dispersion in the records (van der Plicht et al., 2004). Nonetheless, a ^{14}C calibration is still needed and this has led to the development of stand-alone calibrations based on subsets of the available data (Fairbanks et al., 2005; Mellars, 2006; Weninger and Joris, 2008). Some of these are in broad use today, though the ^{14}C community has yet to ratify any one of these for a variety of reasons (Reimer et al., 2006). Critically, the lack of consensus for the pre-26 ka cal BP period undermines efforts to establish the relative timing of important events in both the palaeoenvironmental and archaeological sciences.

Among the potential problems associated with using marine archives for atmospheric $\Delta^{14}\text{C}$ reconstruction is the possibility that the marine reservoir age may have varied in the past. Hence, additional terrestrial records are highly desirable in order to determine the reliability of marine-based ^{14}C records. Stalagmites have been

* Corresponding author. Bristol Isotope Group, University of Bristol, UK.

E-mail addresses: dirk.hoffmann@bristol.ac.uk (D.L. Hoffmann), wbeck@physics.arizona.edu (J.W. Beck), david.richards@bristol.ac.uk (D.A. Richards), p.l.smart@bristol.ac.uk (P.L. Smart), joy.singarayer@bristol.ac.uk (J.S. Singarayer), juniorg1@hotmail.com (T. Ketchmark), c.j.hawkesworth@bristol.ac.uk (C.J. Hawkesworth).

previously proposed for ^{14}C calibration purposes (Beck et al., 2001; Genty et al., 1999; Vogel, 1983; Vogel and Kronfeld, 1997), although these suffer from the possibility of variations in dead carbon fraction (DCF), the component of carbon derived from the host limestone that is devoid of ^{14}C . This problem is analogous to the marine reservoir age which can vary up to 300 a in the Atlantic (Singarayer et al., 2008). Beck et al. (2001) published the first high-resolution attempt to derive past atmospheric radiocarbon concentrations from a U–Th dated stalagmite. They found a reasonably constant DCF when compared to overlapping parts (11–16 ka) of the IntCal98 calibration curve, but also surprisingly elevated (>1000‰) and variable $\Delta^{14}\text{C}$ levels for the period between 45 and 40 ka BP. While similar fluctuations of $\Delta^{14}\text{C}$ had been reported in a foraminifera-based record from the North Atlantic (Voelker et al., 1998), they are inconsistent with estimates based on U–Th dated corals (Fairbanks et al., 2005) and sub-tropical Atlantic foraminifera from the Cariaco Basin (Hughen et al., 2004, 2006). Hence, further work on Bahamas speleothem $\Delta^{14}\text{C}$ records was needed.

Here, we present a new speleothem-based $\Delta^{14}\text{C}$ dataset derived from a submerged Bahamas stalagmite (GB89-25-3), which we believe provides a robust high-resolution terrestrial record of past $\Delta^{14}\text{C}$. We show that the older part of the previous speleothem record (GB89-24-1) was adversely affected by a previously unrecognised ^{14}C blank effect. New measurements on GB89-24-1 using low-blank measurement techniques much more closely resemble coral (Fairbanks et al., 2005), Iberian Margin sediment (Bard et al., 2004c) and Cariaco Basin sediment records (Hughen et al., 2004, 2006). These new GB89-24-1 measurements are also in excellent agreement with the new U–Th dated high-resolution ^{14}C record presented here.

Continuous records of past atmospheric ^{14}C variation, such as that provided by the new speleothem record, enable us to test model results of transient ^{14}C distribution under changing earth system scenarios. We adopt here the intermediate complexity model GENIE-1 (Grid ENabled Integrated Earth system model) (Lenton et al., 2006) to provide comparison model simulations for much of MIS3 and assess the relative influence of changes of geomagnetic field intensities and the ocean–atmosphere system.

2. Site and samples

Stalagmites GB89-25-3 and GB89-24-1 were collected in the shallow underwater cave Sagittarius Blue Hole on Grand Bahama, one of the four northern islands of the Bahamas Archipelago. GB89-24-1 was previously described and analysed for U–Th (TIMS) and AMS ^{14}C in the study by Beck et al. (2001). GB89-25-3 is a candle-stick type stalagmite with a mean diameter of about 5.5 cm that formed at a depth of 15 m below present sea level. Six broken pieces with a total length of 960 mm were recovered, 4 consecutive basal pieces (GB89-25-3-s, t, u, v with a total length of 700 mm) and 2 top section pieces (GB89-25-3-w, x with a total length of 260 mm), the intermediate section being lost during collection. The stalagmite consists of dense crystalline calcite, generally without visible layers, though some oscillations between dense clear calcite and slightly opaque white calcite are observed. There is no evidence of erosion or recrystallisation along the main axis of growth.

3. Methods

3.1. Speleothem sampling

The six sections of speleothem GB89-25-3 were sliced in half along the growth axis and then polished, with one side of each section archived for future reference. Slabs (~5 mm width) were cut from each section either side of the growth axis as shown in Fig. 1 with one slab used for ^{14}C and U–Th sub-sampling. The ^{14}C samples were prepared with a diamond coated wire saw (Well Diamond Wire Saws, Inc.) using cuts of 2 mm depth following the growth layer with a spacing of 1 mm, producing sequential calcite wafers of about 20–

30 mg each. Calcite wafers were used for AMS ^{14}C analysis rather than powdered samples in order to minimise sample surface area and the potential for contamination with adsorbed atmospheric CO_2 . U–Th samples of ~100 mg were similarly cut adjacent to the ^{14}C sample positions and removed from the remaining block as indicated in Fig. 1. We can therefore accurately allocate a distance from base on the central growth axis for all ^{14}C and U–Th sub-samples. Six U–Th samples of the topmost piece GB89-25-3x were prepared as powder samples using a handheld drill. To assess the influence of initial ^{230}Th on age determinations, we also performed three U–Th isochron analyses, each based on 7 drilled powder sub-samples, for well defined layers from the topmost section.

For this study a new set of 14 calcite wafers was also taken from the bottom section of GB89-24-1 (Beck et al., 2001) and analysed for AMS ^{14}C using new low-blank protocols. The samples cover the time interval 44–41 ka BP that previously yielded dramatic shifts in $\Delta^{14}\text{C}$ (Beck et al., 2001).

3.2. U–Th sample preparation

Calcite wafers of 50–150 mg were leached for a few seconds in weak (<0.1 N) HNO_3 to remove potential surface contamination or residuals from the cutting process, immediately rinsed in a MQ H_2O ultrasound bath and dried. After weighing, the samples were placed in a Teflon beaker, MQ H_2O was added and then carefully dissolved by stepwise addition of 7 N HNO_3 . A mixed $^{229}\text{Th}/^{236}\text{U}$ spike was added and the solution evaporated to dryness for sample–spike equilibration. Organic components were decomposed by refluxing the samples in a combination of concentrated HNO_3 , HCl and H_2O_2 . After the sample was dried down again, the residual was dissolved in 6 N HCl and processed through ion exchange resin (pre cleaned AG 1x8) to separate Th (passes through) and U fraction (eluted with 1 N HBr followed by MQ H_2O). The two fractions were evaporated to dryness, taken up in 7 N HNO_3 and separately passed through the ion exchange resin for purification. Th is eluted with 6 N HCl and U is eluted with 1 N HBr followed by MQ H_2O . The pure U and Th fractions were finally taken up in 0.6 N HCl for MC-ICPMS measurements.

3.3. U–Th measurements and age model

Analytical procedures used at the Bristol Isotope Group (BIG) laboratory for U and Th isotope measurements are reported in full in Hoffmann et al. (2007). In brief, U-series isotope measurements were undertaken using a ThermoFinnigan Neptune multi collector inductively coupled plasma mass spectrometer (MC-ICPMS). The sample introduction system consists of a Cetac Aridus nebulizer equipped with a PFA spray chamber and a heated desolvating membrane. A nebulizer tip with a nominal uptake rate of $50 \mu\text{l min}^{-1}$ was used for

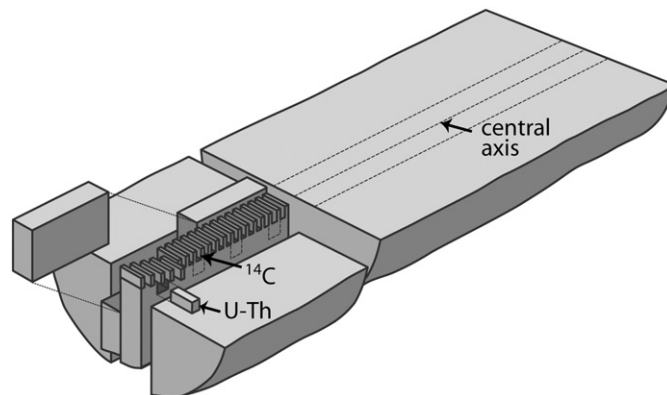


Fig. 1. Idealised sub-sampling scheme for ^{14}C and U–Th determinations from one half of a stalagmite piece. See text for details.

sample introduction. U and Th fractions are routinely measured separately in a 0.6 N HCl solution. A standard-sample bracketing procedure is adopted to derive correction factors for mass fractionation and Faraday cup to SEM gain. For U measurements we use NBL-112a as the bracketing U-standard. Thorium measurements are bracketed with an in-house ^{229}Th – ^{230}Th – ^{232}Th Th-standard (TEDDi). U–Th activity ratios are calculated using the ^{230}Th and ^{234}U half-lives reported in Cheng et al. (2000), the ^{238}U half-life given in Jaffey et al. (1971) and the ^{232}Th half-life reported in Holden (1990). All uncertainties are propagated as described in Hoffmann et al. (2007) and quoted at 95% confidence limit, unless otherwise stated.

A distance–age model for the central axis of the stalagmite was generated using a smoothing cubic spline. Our algorithm uses the smooth.spline function of open source statistical software R (<http://www.r-project.org>) to derive a spline fit and associated 95% confidence intervals. The fit is based on all the U–Th ages and their uncertainties for the speleothem. Where there are significant cessations in growth, the spline is developed for individual growth sections. Weights for each predictor value are based on the inverse of the associated variance, where age uncertainty is quoted at 95% confidence limits. As a starting point an automatic derivation of the smoothing parameter and equivalent degrees of freedom (*df*) is used. A boundary condition is set by the monotonicity of the distance–age model. Thus, for cases where an automatic spline fit based on the generalised cross validation technique produces an age model with roughness resulting in age inversions, *df* is restricted to the maximum value that maintains monotonicity.

3.4. ^{14}C AMS sample preparation

A thorough analysis of the sources and variability of accelerator mass spectrometry (AMS) ^{14}C procedural blanks during sample processing for low- ^{14}C -abundance (old) samples has caused us to revise sample handling and blank subtraction procedures at the University of Arizona NSF AMS facility. Previously, speleothem samples were processed using standard hydrolysis protocols and standard vacuum-line equipment used for general sample processing. However, we have found that this equipment and procedures introduced a higher and more variable processing blank than previously thought, which is significant for older samples. Large sample sizes have been used in this and the previous study (Beck et al., 2001) in an effort to minimise procedural blanks during sample processing. A careful evaluation of the processing blank for large sample sizes has shown that the simple inverse mass equation observed for sample sizes of less than 1 mg and used in the previous speleothem study (Beck et al., 2001) does not adequately correct for processing blank for large sample masses (>1 mg carbon). Finally, we found that non-random temporal variability in the procedural blank, in combination with the unfortunate practice of analysing samples in chronological order introduced aliasing resulting in erroneous structure in the ^{14}C results of the previous publication of Bahamas speleothem ^{14}C measurements (Beck et al., 2001), especially for samples older than 40 ka radiocarbon age. Blank subtraction procedures and processing order have been revised accordingly in the present study.

Sample preparation for AMS ^{14}C measurements in the present study were conducted using new protocols for low- ^{14}C -abundance (old) samples, and a new low-level sample preparation vacuum-line and graphitisation system dedicated to low- ^{14}C -abundance sample processing only (Pigati et al., 2007). Only samples older than 25 kyr uncalibrated radiocarbon age are processed in these vacuum systems, to help minimise cross-contamination from samples of young age. Other special procedures have also been implemented to minimise contamination with young carbon. Among these are

- oxidation then reduction of Zn/Fe reagents used for graphitization prior to introduction of sample CO_2 ;
 - repeated purging with 99.999% purity He and heat treatment of processing lines between samples,
 - new protocols designed to minimise cross-contamination and sample contamination with young carbon.
- In addition procedural blanks have been run at high frequency (1 every 6 samples) to characterise non-random variations in the blank. Only random variations were observed using the new equipment and protocols. Blanks analysed using these new protocols and equipment are found to vary inversely with mass below 1 mg sample size, and to be constant above this level. The average blank in this study is found to be $1.11 \pm 0.35\%$ ($N = 22$), equivalent to a radiocarbon age of 54,600 (+3000, –2180) yr.

3.5. AMS ^{14}C measurements

AMS ^{14}C measurements for this study were all made using a National Electrostatics Corporation (NEC)-based AMS system, comprised of a caesium sputter negative ion source, a 90° injection magnet with high-speed electrostatic bouncing of carbon isotopes, a 3.0 MV tandem accelerator with gas stripper, followed by a quadrupole doublet lens, a 15° cylindrical electrostatic analyser for charge state selection, a high-energy 90° analysis magnet with $\text{ME}/q^2 = 176$, a 2.0 m radius 77° spherical electrostatic analyser to enhance abundance sensitivity, a 22° beam line switching magnet, followed by a silicon surface barrier detector ion-counting system.

Measurements were made at 2.5 MV terminal voltage with typical ion source $^{12}\text{C}^-$ ion beam currents of 60–70 μA after the injection magnet, and 49–51% C^{3+} charge state transmission after the terminal. $^{13}\text{C}^{3+}$ currents are measured by Faraday cup following the high-energy analysis magnet, whereas the $^{14}\text{C}^{3+}$ beam is measured at the surface barrier detector. A correction for stable isotope fractionation is applied to AMS $^{14}\text{C}/^{13}\text{C}$ measurements using off-line $^{13}\text{C}/^{12}\text{C}$ measurements with a Fisons Optima mass spectrometer with dual inlet. The average machine blank $^{14}\text{C}/^{13}\text{C}$ based on SP-1 reagent grade graphite is 7.5×10^{-16} , corresponding to radiocarbon age of 59,100 yr. Error analysis for AMS measurements include terms for counting statistics uncertainty, measurement scatter error, uncertainty in the blank correction, and a random machine error term based on the six-month average daily reproducibility of eight OX1 and OX2 standards loaded in every wheel of sample targets (Burr et al., 2007). Uncertainty in calculated speleothem $\Delta^{14}\text{C}$ also includes terms for uncertainty in the U–Th age model generated by the roughness penalty approach (see above), and uncertainty in DCF (see below) as determined from comparison between stalagmite and INTCAL04 $\Delta^{14}\text{C}$ for the period 11–15 ka BP.

3.6. The GENIE model

The Grid ENabled Integrated Earth system model (GENIE-1) consists of a fully-dynamic 3-D ocean, 2-D energy and moisture balance atmosphere and sea-ice, as well as terrestrial, ocean, and sediment carbon cycle components (Lenton et al., 2006; Ridgwell et al., 2007; Williamson et al., 2006) to allow closure of the carbon cycle. The model is forced with the scalar annual average wind speed (Trenberth et al., 1989). It has been calibrated against present-day observations using a multi-objective tuning process (Price et al., 2006). The physical climate is optimised using targets from observational data of surface air temperature and humidity, and 3D ocean temperature and salinity. The model resolution chosen was 36 by 36 equal area grid cells with 16 vertical ocean levels.

Stable (^{12}C , ^{13}C) and radio- (^{14}C) isotopes of carbon and their processes of fractionation are treated explicitly in the model. Fractionation occurs during terrestrial photosynthesis, within the

aqueous carbonate system, and during air–sea gas exchange and ocean biological productivity (Ridgwell et al., 2007). Cosmogenic production of ^{14}C is calculated as a time-varying function of geomagnetic intensity, given by Eq. (1) (Elsasser et al., 1956),

$$P/P_0 = \sqrt{1/M/M_0} \quad (1)$$

where P is the time-varying ^{14}C production rate, P_0 is present-day production rate, M is the time-varying global geomagnetic intensity and M_0 is present geomagnetic intensity. This simplified relationship between geomagnetic intensity and global ^{14}C production can be used for geomagnetic intensity that is >20% of present intensity (Bard, 1998). The addition of newly produced ^{14}C is distributed uniformly over all atmosphere grid cells, under the assumption that ^{14}C is relatively homogeneous when it reaches the lower atmosphere. P_0 was set to $1.6 \text{ atoms cm}^{-2} \text{ s}^{-1}$, based on comparison of the model with the present-day radiocarbon inventory. This is similar to other modelling studies (e.g. Meissner et al. (2003)), but is at the lower end of 20th century production rate estimates.

The GENIE-1 modelled radiocarbon ocean distribution was evaluated against present-day ‘natural’ ^{14}C and penetration of ‘bomb’ ^{14}C using a similar method to the Ocean Carbon Cycle Model Intercomparison Project (OCMIP) (Matsumoto et al., 2004), in which 19 different models were assessed. The GENIE-1 model proved better than 75% of the OCMIP models, when compared to observational data (Singarayer et al., 2008).

The model was spun-up to equilibrium for 40,000 yr with 50 ka BP fixed boundary conditions. These include 50 ka estimated ice sheet extent and orbit (Marsh et al., 2006). Atmospheric CO_2 was prescribed at 220 ppmv (Petit et al., 1999) and relative geomagnetic intensity, $M/M_0 = 1$ (Laj et al., 2004). Following the initial spin-up, the model was run with transient boundary conditions from 50 ka BP to 25 ka BP. During the transient runs all carbon isotopes were allowed to vary in response to transient climate change. Three model simulations of $\Delta^{14}\text{C}$ are presented in this study:

1. Changing geomagnetic intensity based on GLOPIS (Laj et al., 2004) and insolation changes and ice sheet configuration following Marsh et al. (2006). Fig. 2 a,b shows the model prescribed ice sheet extent at two time slices (50 ka BP and 25 ka BP).
2. As above, but to evaluate the impact of changing ocean circulation patterns on the structure of $\Delta^{14}\text{C}_{\text{atm}}$, we imposed periodic freshwater inputs to the model to simulate Heinrich events. We use triangular pulses, maximum 0.3 Sv, 500 a duration at H4 (40 ka) max 0.15 Sv, 500 a at H3 (29.5 ka).
3. As in 1 and 2 with additional ‘sea-ice’ variability in Southern Ocean. We know that sea ice extent was seasonally much greater during glacial times and this is not well simulated by GENIE, so we increase salinity (simulating brine rejection) in circum Antarctic grid cells (with balancing freshwater melt to maintain global salinity balance). This has the effect of decreasing North Atlantic Deepwater (NADW) and increasing Antarctic Bottom Water (AABW) (as observed in $\delta^{13}\text{C}$ transect for this period). The structure and magnitude of this forcing is linearly related to EPICA δD (Jouzel et al., 2007) as a proxy for Antarctic temperatures.

4. Results

4.1. U–Th chronology for GB89-25-3

Stalagmite GB89-25-3 is composed of dense non-porous polycrystalline calcite and is mostly free from detrital contamination. The ^{232}Th concentration in GB89-25-3 is generally very low (<0.5 ng/g). For 26 of 45 samples from the basal section and 21 of 35 samples from the upper section no ^{232}Th was detectable. Samples with detectable

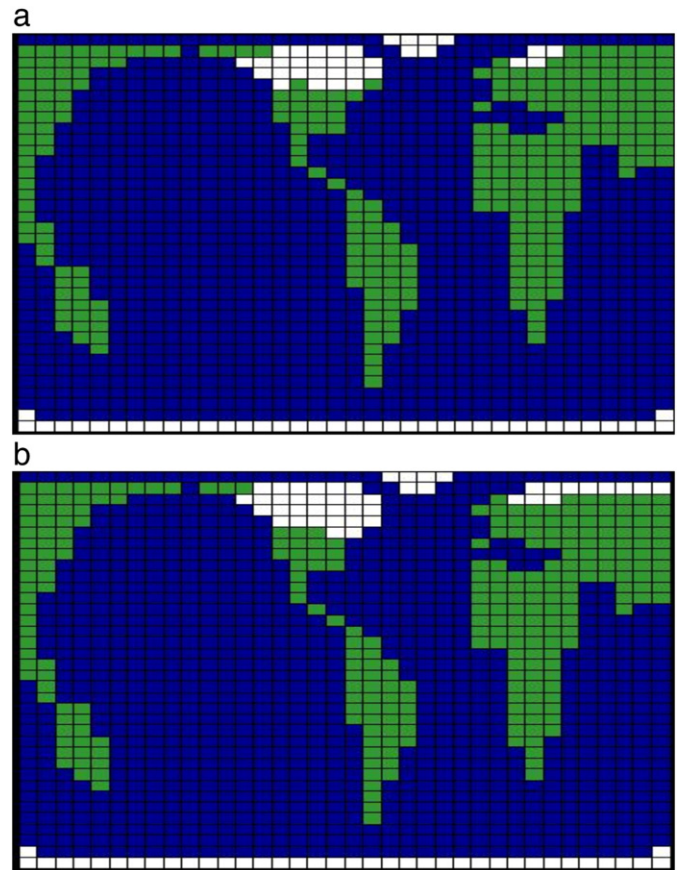


Fig. 2. Example ice sheet extent prescribed in GENIE-1 simulations for the time 50 ka (a) and 25 ka (b) BP.

^{232}Th all have $^{230}\text{Th}/^{232}\text{Th}$ activity ratios greater than 200. Nevertheless, isochron analyses were performed to determine initial $^{230}\text{Th}/^{232}\text{Th}$ ratio on one of the two upper sections where relatively high ^{232}Th concentrations and clearly visible growth layers are detected. Three isochrons yield a mean initial $^{230}\text{Th}/^{232}\text{Th}$ activity ratio of 7.8 ± 4.0 . This is an elevated initial $^{230}\text{Th}/^{232}\text{Th}$ ratio compared to a value of 0.8 for the upper crust (Wedepohl, 1995) for which we assume an arbitrary uncertainty of 50%. Beck et al. (2001) reported an even more elevated ratio of 18.7 ± 2.9 for stalagmite GB89-24-1 from the same cave. An initial ratio of 7.8 ± 4.0 is used for correction of all GB89-25-3 samples where ^{232}Th was detected. In Supplementary Tables 3 and 4 both the uncorrected and ^{232}Th corrected results are reported together with all other U and Th data. The isochron data are reported in Supplementary Table 5.

The U concentration of GB89-25-3 ranges between 60 and 360 ng/g. For all but the last 3 mm of the basal section, U–Th ages of solid wafers from the central axis reveal continuous growth between 44 and 28 ka BP (Fig. 3b). There is a single age of 23.8 ± 0.2 ka above an apparent growth hiatus at the top of the basal section indicating a hiatus from 27.7 ± 0.2 to 23.8 ± 0.2 ka. Thirty-five U–Th ages (29 solid wafers and 6 drilled powder samples) from the upper section reveal ages between 15 and 11 ka.

The distance–age models of GB89-25-3 were developed separately for the two sections separated by a hiatus of significant duration, based on 44 (basal) and 35 (upper) MC-ICPMS U–Th dates. Fig. 3a and b shows the U–Th dating results together with the spline fit and the 95% confidence band for the age model. We obtain equivalent degrees of freedom of $df=21$ (automatic, basal section) and $df=10$ (restricted, upper section). Mean growth rates of the basal and upper sections are 0.05 and 0.09 mm/a, respectively. The modelled

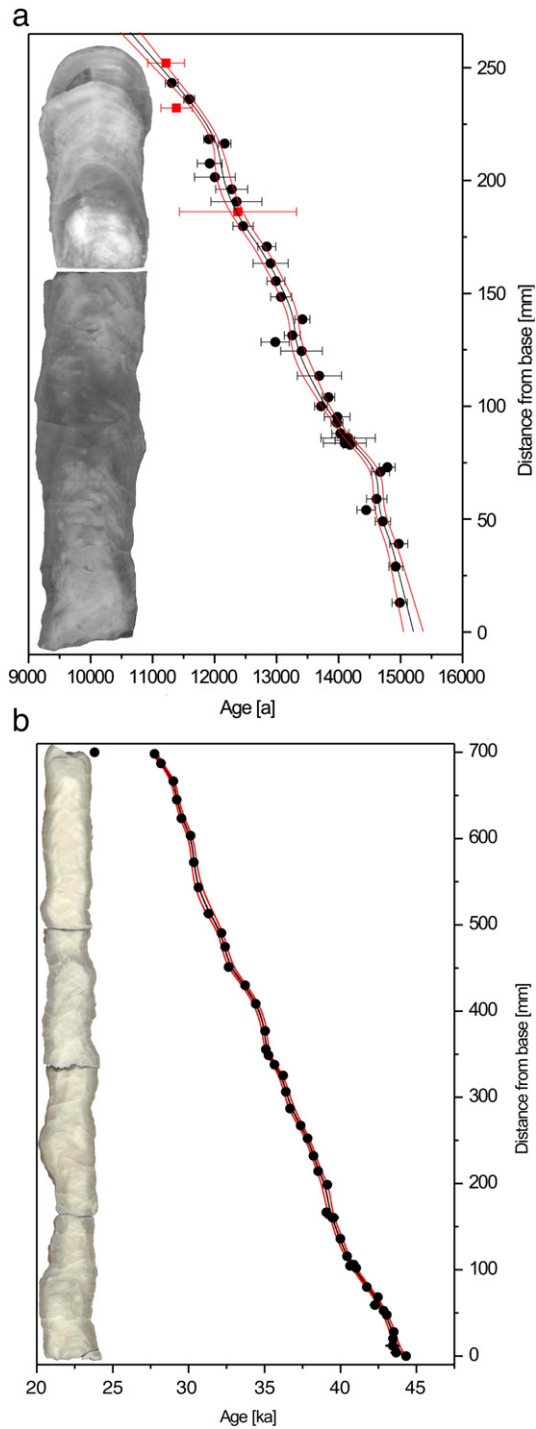


Fig. 3. U–Th dating results of GB89-25-3 against distance from base and weighted cubic spline age model (black line) for the top (a) and basal (b) sections. Red lines indicate the 95% confidence limits of the cubic spline fit. For the basal section most error bars of U–Th ages are within the symbols. The red symbols in (a) are isochron ages.

growth rates change between 0.024–0.145 mm/a (basal section) and 0.03 – 0.26 mm/a (upper section).

4.2. Assessment of dead carbon fraction (DCF)

Radiocarbon ages have to be corrected for DCF in drip waters that results in ‘apparent’ ^{14}C ages of precipitated calcite older than the ‘true’

^{14}C age. This effect is analogous to that of a marine reservoir age on the apparent ^{14}C age of marine carbonates. Beck et al. (2001) demonstrated a reasonably constant DCF offset for the stalagmite GB89-24-1 by comparing apparent ^{14}C ages with the then-current IntCal98 calibration curve (Stuiver et al., 1998) for the period 15.5 to 11.1 ka. Following Beck et al. (2001), we assess the extent of DCF in the stalagmite GB89-25-3 based on a comparison of radiocarbon ages with the more recent IntCal04 calibration curve (Reimer et al., 2004) for the overlapping period at 15 to 11 ka. Fig. 4a shows the GB89-25-3 ^{14}C ages of the upper and basal sections together with the IntCal04 data that cover the time back to 26 ka. The age offset of the upper section is found to be reasonably constant with a mean value of 2075 ± 540 a (Fig. 4b). There is a non-random structure in the DCF corrected GB89-25-3 data compared to the IntCal04 curve, especially between 12.8 and 11.2 ka, which is reflected in the rather large uncertainty of the DCF estimate. We conservatively assume the residuals are a combination of minor changes in DCF and measurement error associated with the GB89-25-3 record and not due to errors in the IntCal04 calibration curve. We thus use the 2σ standard deviation (± 540 a) instead of the smaller standard error of the mean to represent the uncertainty of the DCF correction applied to ^{14}C ages older than 28 ka. Fig. 4b also shows the DCF corrected ^{14}C ages of GB89-24-1 published in Beck et al. (2001). The similarity of the two estimates for different samples from the same cave gives us confidence that the younger sections, both processed with the original methods, are not significantly affected by blank effects.

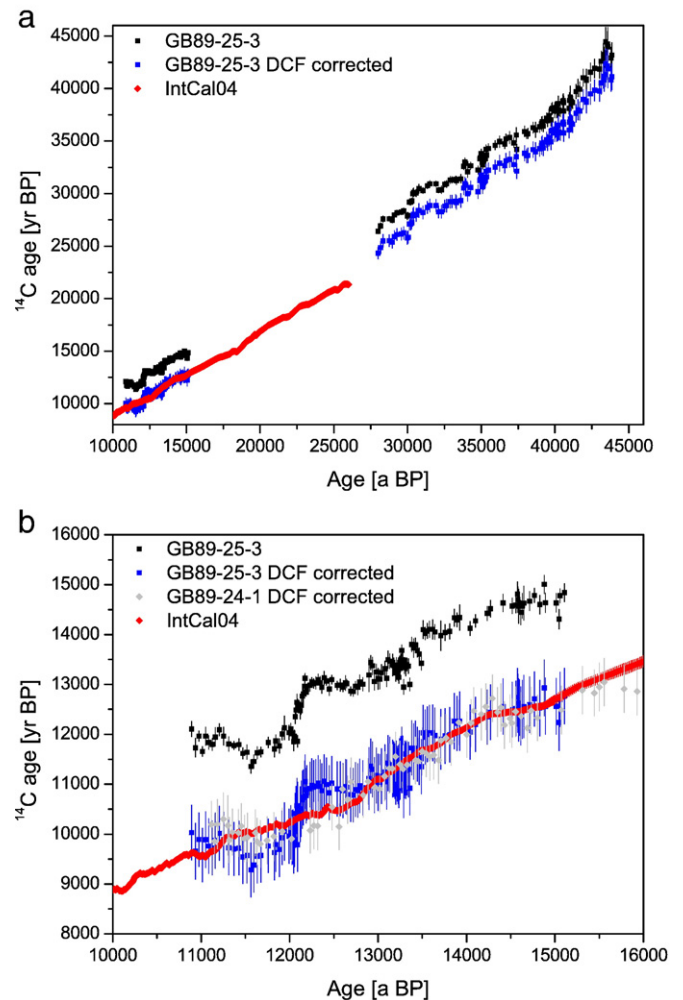


Fig. 4. a, b. ^{14}C ages of GB89-25-3 uncorrected (black) and corrected (dark blue) for DCF (2075 a). Red are IntCal04 ^{14}C age data (Reimer et al., 2004) and light blue DCF corrected ^{14}C ages of GB89-24-1 (Beck et al., 2001).

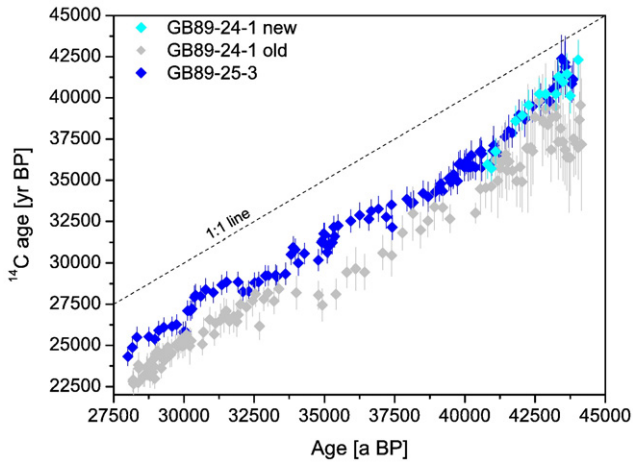


Fig. 5. ^{14}C ages of stalagmite GB89-25-3 and new ^{14}C ages obtained for GB89-24-1 between 44 and 41 ka BP. The previously published ^{14}C ages of GB89-24-1 (Beck et al., 2001) is also shown for comparison.

4.3. ^{14}C results for GB89-25-3 and GB89-24-1

Fig. 5 shows the DCF corrected ^{14}C ages of GB89-25-3 covering the time between 44 and 28 ka BP together with 14 newly measured ^{14}C ages of GB89-24-1 in the oldest section between 44 and 41 ka BP and the previously published ^{14}C ages of GB89-24-1 (Beck et al., 2001). The striking similarity between the two new stalagmite records, which are U–Th dated in two different laboratories and have different DCF leads us to place confidence in the new speleothem ^{14}C data. This also suggests that blank problems have been resolved by the new low-blank ^{14}C preparation procedures. The comparison to the old GB89-24-1 data in Fig. 5 shows the significance and size of discrepancy of our new ^{14}C results for the whole period between 44 and 28 ka and especially between 44 and 40 ka. Converting the new data to $\Delta^{14}\text{C}$ (Fig. 6) we now find $\Delta^{14}\text{C}$ excursions between 44 and 41 ka to be much smaller than previously described in Beck et al. (2001),

although substantial variation is still observed. For example, between 44 and 41 ka $\Delta^{14}\text{C}$ increases from 0 to 600‰, followed by a decreasing trend to 300‰ until 36 ka with a small peak around 39 ka. Between 36 and 35 ka $\Delta^{14}\text{C}$ shows another peak and increases from 300 to 500‰, and similarly between 31 and 30 ka from 200 to 400‰. All ^{14}C results are reported in Supplementary Tables 1 and 2.

4.4. GENIE model results

To investigate the relative influence of geomagnetic and ocean-system changes on atmospheric $\Delta^{14}\text{C}$, we have used the ^{14}C isotope-enabled intermediate complexity model GENIE-1 along with the stacked reconstruction of geomagnetic palaeointensity GLOPIS (Laj et al., 2004), for which we also used the GICC05 timescale (Svensson et al., 2008) rather than the original GISP2 chronology (Meese et al., 1997). The results of three atmospheric $\Delta^{14}\text{C}$ reconstructions, one with modern ocean dynamics and the others with different configurations of overturning circulation and sea ice cover reveal very similar $\Delta^{14}\text{C}$ structure to that observed in stalagmite GB89-25-3 (Fig. 6).

The model results largely reflect the virtual axial dipole moment (VADM) of the GLOPIS dataset (Laj et al., 2004) and suggest that major $\Delta^{14}\text{C}$ fluctuations are primarily a result of variations in the geomagnetic palaeointensity and that changes in North Atlantic circulation produced only second order effects. The model results describe all the major $\Delta^{14}\text{C}$ increases found for the speleothem record. However, the model results and speleothem data notably diverge between 34 and 32 ka where the speleothem $\Delta^{14}\text{C}$ values remain elevated at 400–500‰ whereas the model predicts decreasing $\Delta^{14}\text{C}$.

5. Discussion

5.1. Bahamas speleothem ^{14}C ages

Accuracy of past atmospheric $\Delta^{14}\text{C}$ reconstruction based on speleothems critically depends on a reliable DCF correction. We therefore reassess and discuss our approach to establish a constant

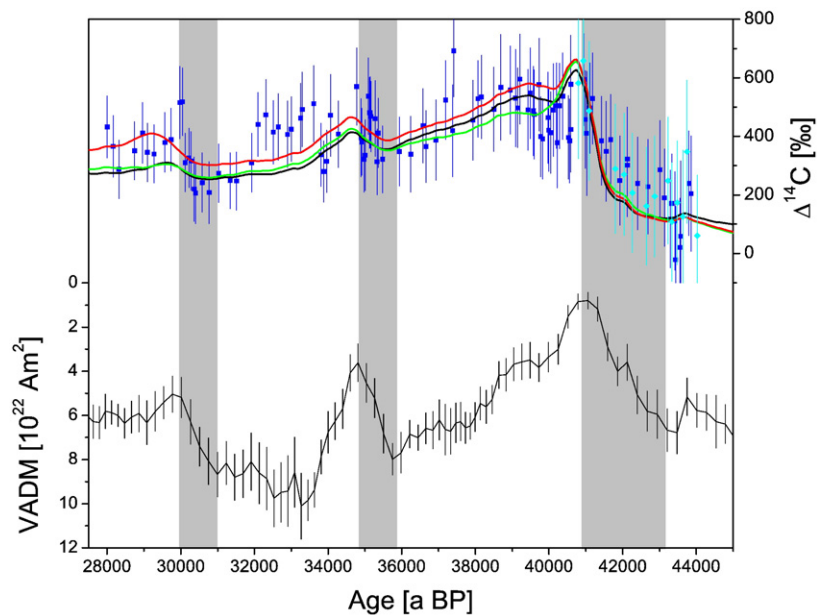


Fig. 6. top: $\Delta^{14}\text{C}$ from GB89-25-3 (blue) and GB89-24-1 (cyan) compared to earth system model simulations. We illustrate here three model simulations of atmospheric $\Delta^{14}\text{C}$ from 45 to 28 ka. Simulation 1 (green) includes only transient changes in geomagnetic intensity from the GLOPIS dataset (Laj et al., 2004), ice sheet extent, and orbital parameters. Simulation 2 (black) includes in addition Heinrich events H4 and H3. Simulation 3 (red) additionally uses a time-varying Southern Ocean salinity flux to represent increased extent of sea-ice during the glacial. See text for details. bottom: GLOPIS proxy for palaeo magnetic intensity given as virtual axial dipole moment (VADM) (Laj et al., 2004) using GICC05 chronology. Grey bars indicate times of decreasing magnetic palaeointensity resulting in increasing $\Delta^{14}\text{C}$.

DCF, which is used to correct ^{14}C results for sections older than 28 ka. We obtain the same DCF corrected ^{14}C age results for the two stalagmites between 44 – 40 ka using the DCF individually established on the overlap with IntCal, indicating that this approach is robust for speleothems from this cave. However, local effects which are similar for all speleothems from the same cave cannot be excluded. The comparison of stalagmite ^{14}C ages to IntCal04 (Reimer et al., 2004) between 15 and 11 ka shows similar trends but also some significant differences (Fig. 4b). The most significant and apparently non-random difference between IntCal04 and the stalagmite record is found to be synchronous with the time of the Younger Dryas (YD), a period with abrupt major changes in the global climate system. The apparent DCF is variable between 15 and 29% during this period of dramatic climatic transitions when vegetation and climatic conditions changed significantly. However, we established a mean offset of $2075 \pm 540\text{a}$ to IntCal 04 which corresponds to a DCF of $22.7 \pm 5.9\%$. Our result of a near constant DCF is supported by other studies that also find that temporal variations of DCF are small in speleothems (Jackson et al. (2008); both Arabian and Bahamas speleothems included in NotCal (van der Plicht et al., 2004)). A comparison of our speleothem derived ^{14}C results to marine-based ^{14}C age data sets such as the foraminifera records from Iberian Margin (Bard et al., 2004a,c; Shackleton et al., 2004) and the Cariaco Basin (Hughen et al., 2006) for the period of the Heinrich Event 4 (H4) does not indicate significant variations similar to YD in the older section (Fig. 7). We therefore argue that local DCF was not significantly variable during the time 44–28 ka.

While we have assumed here that the difference to IntCal04 during the YD is a pure local effect, there is a possibility that these deviations may in part reflect real changes in the atmospheric $\Delta^{14}\text{C}$ not present in the IntCal04 curve, which is based on marine records for this period. This possibility is supported by the work of Muscheler et al. (2008) who recently demonstrated that the IntCal04 ^{14}C ages between 13 and 12.5 ka are probably too young, bringing them to closer agreement with the speleothem results presented in this study. If correct, the deviation of our speleothem data from the IntCal04 curve may not entirely be due to local DCF variations. Nevertheless, until an updated version of IntCal is available, we continue to use IntCal04 to establish DCF in our speleothem record and we use the standard deviation from the mean IntCal offset instead of standard error as an uncertainty term for correcting ^{14}C results of the older section.

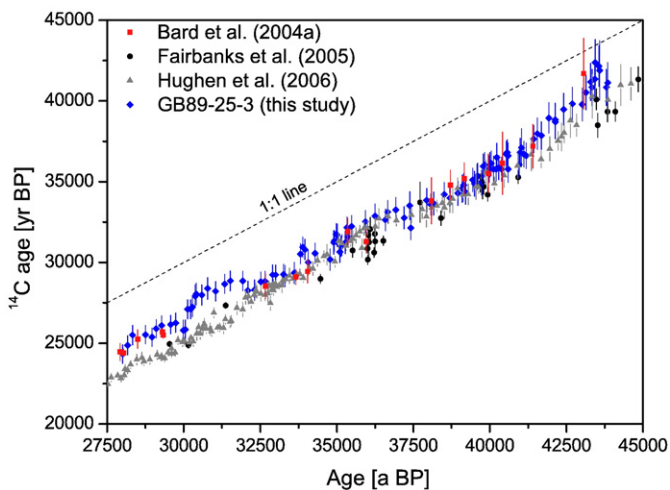


Fig. 7. ^{14}C age vs. calendar age scatter-plot for GB89-25-3 for the time 44 – 28 ka and marine ^{14}C data sets, derived from foraminifera from the Cariaco Basin (Hughen et al., 2006) and Iberian Margin (Bard et al., 2004a) and from corals from the Pacific Ocean (Fairbanks et al., 2005). The Cariaco Basin ^{14}C ages are based on the assumption of a constant reservoir age of 400 yr and the coral data are corrected using 365 yr. GB89-25-3 ^{14}C ages are corrected for a DCF of 2075 yr.

Our new high-resolution speleothem data set has many of the same features as those for the current version of the most continuous alternative ^{14}C data set from the Cariaco Basin, except for the periods 41–43 ka BP and, most notably, 28–32 ka BP (Fig. 7). However, the more sparse Iberian Margin record (Bard et al., 2004a) shows good agreement with the speleothem record over the full time span of 44 – 28 ka. The coral data set (Fairbanks et al., 2005), which was recently suggested as a stand-alone ^{14}C calibration curve, is too sparse to compare features. It generally agrees with the speleothem and foraminifera data sets, but with systematically younger radiocarbon ages. This offset could be a result of incorrect marine reservoir age or could be explained if the coral samples were contaminated by overgrowths of younger diagenetic aragonite, a phenomenon observed in other subaerially exposed corals used for radiocarbon calibration (Burr et al., 1992). The large spread in the coral data observed at ~36 ka BP hints at a possible problem of this nature (Fig. 7), but at present, we cannot choose between these possible explanations.

5.2. $\Delta^{14}\text{C}$ variability at 44–28 ka

Our speleothem $\Delta^{14}\text{C}$ record together with model results (Fig. 6) strongly indicate that the Earth's magnetic field is primarily responsible for modulation of $\Delta^{14}\text{C}$ at millennial timescales. The most dramatic $\Delta^{14}\text{C}$ increase (>500‰) occurs between 44 and 41 ka, and is matched by a contemporaneous drop in virtual axial dipole moment (VADM), which fell to near zero at ~41 ka. The timing of this $\Delta^{14}\text{C}$ peak matches that determined for the well-known Laschamp geomagnetic excursion with an assigned Ar–Ar age of $40.4 \pm 2.0\text{ ka}$ (Guillou et al., 2004) and the related ^{10}Be peaks observed in Summit ice cores from Greenland (Muscheler et al., 2005) and in ocean cores from the Portuguese Margin (Carcaillet et al., 2004) and western equatorial Pacific (Leduc et al., 2006). Two later steep $\Delta^{14}\text{C}$ rises in GB89-25-3 are also matched by concomitant drops in the GLOPIS geomagnetic intensity record (Laj et al., 2004) at about 35 ka and 30 ka. Although our model results clearly show that geomagnetic field variations are primarily responsible for the features observed in our record, ocean–atmosphere reorganisation may account for some of the structure we see in the $\Delta^{14}\text{C}$ record. For example, the double peak between 41 and 39 ka may be a result of circulation-related increases in $\Delta^{14}\text{C}$ related to H4, superimposed on larger increases caused by reduced geomagnetic field strength.

While much of the structure observed in GB89-25-3 is reproduced by model simulations, some of the structure is not. Most interesting is a disparity at 34–32 ka, where there is excellent agreement between the speleothem and Cariaco Basin foraminifera data. We speculate that a Heinrich-type climate event with changes in the ocean circulation system might be a possible explanation, or that the structure of the Mono Lake geomagnetic excursion at ~35 ka BP is more complex than that revealed by the smoothed stacked GLOPIS record.

Agreement between our speleothem record and the Cariaco Basin record can be substantially improved, especially between 28 and 32 ka BP, if the calendar age model used for the Cariaco data set is adjusted to the new Greenland ice core chronology (GICC05) (Svensson et al., 2008). In 2006, the calendar age timescale for the Cariaco record was revised (Hughen et al., 2006) from one based on the GISP2 timescale (Meese et al., 1997) to one based on correlation with the Hulu cave speleothem $\Delta^{18}\text{O}$ record (Wang et al., 2001), and we suggest the observed mismatch may be an artefact related to this revision. We illustrate this problem in Fig. 8 by comparing our $\Delta^{14}\text{C}$ results for the interval 44 to 28 ka with the Cariaco Basin record based on three different timescales: GISP2 (Hughen et al., 2004; Meese et al., 1997), Hulu (Hughen et al., 2006; Wang et al., 2001) and the recently proposed GICC05 Greenland icecore timescale (Svensson et al., 2008). For archives such as that from the Cariaco Basin that are not directly dated and rely for their chronology on matching a signal presumed to

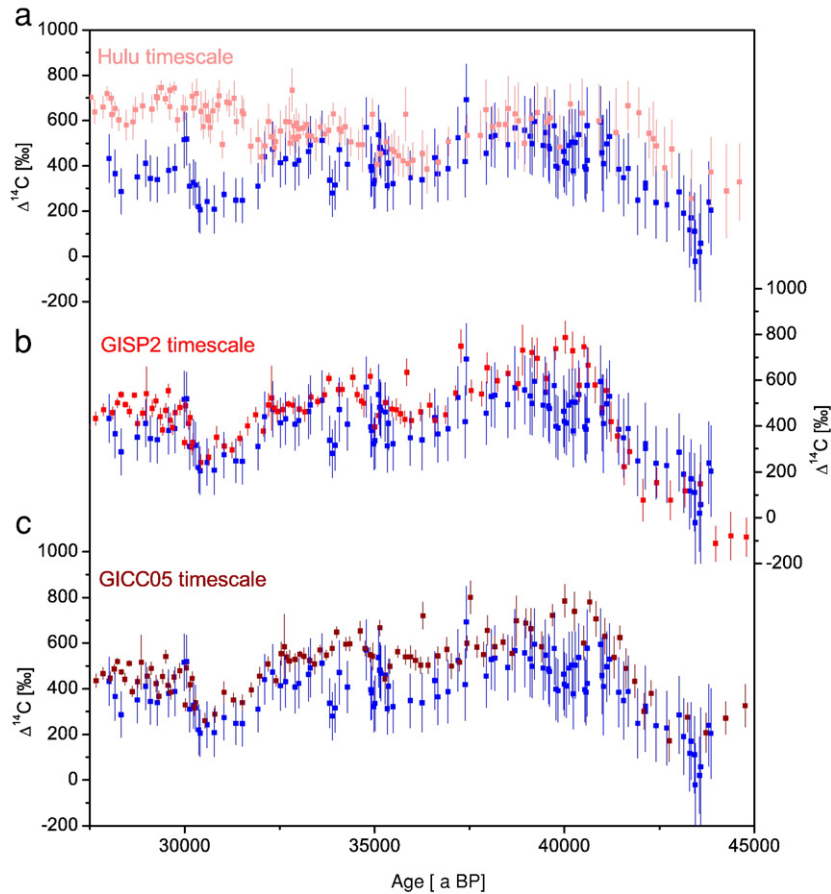


Fig. 8. a) Bahamas speleothem $\Delta^{14}\text{C}$ record GB89-25-3 (blue) compared with the foraminifera record from the Cariaco Basin using Hulu timescale (light red), b) GB89-25-3 (blue) compared to the Cariaco Basin record using GISP2 timescale (red), c) GB89-25-3 (blue) compared to the Cariaco Basin record using GICC05 timescale (dark red).

be synchronous in an alternative archive, calculated $\Delta^{14}\text{C}$ can change substantially for a specific time in the past if the chronology of the correlative record is amended (Hughen et al., 2006). As Fig. 8 shows, there is a much greater similarity between the Bahamas data and that of Cariaco Basin using the ice core chronologies, than for Cariaco using the Hulu-based timescale most recently advocated (Hughen et al., 2006). The latter systematically overestimates $\Delta^{14}\text{C}$ compared to the Bahamas speleothem record, particularly in the intervals 43–41 and 33–28 ka. In contrast, both ice core chronologies show remarkably good coherence with the speleothem record especially with regards to the timing of abrupt changes in slope. The superior concordance between the speleothem and Cariaco records on the GICC05 ice core chronology lends credence to this chronology, and suggests that the recent conversion of the Cariaco Basin data to the Hulu timescale or the Hulu chronology itself needs reassessment. A discrepancy of the Hulu chronology is also found around 31 ka compared to the Botuvera speleothem record (Wang et al., 2006), pointing at least partly towards a chronology problem of the Hulu record for this time interval.

Although the general coherence between marine and speleothem $\Delta^{14}\text{C}$ records observed in Fig. 8c is encouraging, we still find systematic differences in atmospheric $\Delta^{14}\text{C}$ derived from these two records. The Cariaco record generally reveals 50–100% higher atmospheric $\Delta^{14}\text{C}$ than the stalagmite record, except for the period 41–44 ka BP, where the two records are very similar. These differences are likely to be related to variations in one, or a combination, of DCF and the marine reservoir effect, affecting speleothem and the Cariaco records respectively. For GB89-25-3, variation in vegetation, hydrology and geochemistry of the soil and unsaturated zone, may all have influenced the magnitude of

DCF. Likewise, the marine reservoir age in the Cariaco Basin is likely to have been affected by transient changes in ocean circulation patterns and air–sea exchange rates. This view is supported by results of ^{14}C measurements on floating tree rings (Muscheler et al., 2008) and climate models of intermediate complexity under conditions of changing ^{14}C production rates and reduced Atlantic meridional overturning circulation (AMOC) (Singarayer et al., 2008).

5.3. Implications for a ^{14}C calibration curve

At the time of construction of the most recent community-ratified radiocarbon calibration IntCal04 (Reimer et al., 2004), it was declared that the disparities between the available ^{14}C archives older than 26 ka BP were sufficiently large as to preclude promotion of a single calibration curve for this time period (van der Plicht et al., 2004). However, the urgent need to resolve important scientific questions in this time range has nevertheless driven several independent attempts to establish an age calibration (Anikovitch et al., 2007; Gravina et al., 2005; Mellars, 2006). Amongst those now commonly used are the “Fairbanks calibration curve” (Fairbanks et al., 2005), the Cariaco Basin foraminifera record (Hughen et al., 2004, 2006) and a “mean NotCal curve” (Mellars, 2006) that ignores the wide range in ^{14}C ages exhibited by this compilation data set (van der Plicht et al., 2004).

We note that these various archives can produce a difference of up to 1500 a for calibrated radiocarbon ages depending on which calibration curve is used, a range much larger than the uncertainty produced by any single calibration. This has important implications for dating archaeological findings for the period of the transition from Middle to Upper Palaeolithic and the arrival of modern humans in Europe.

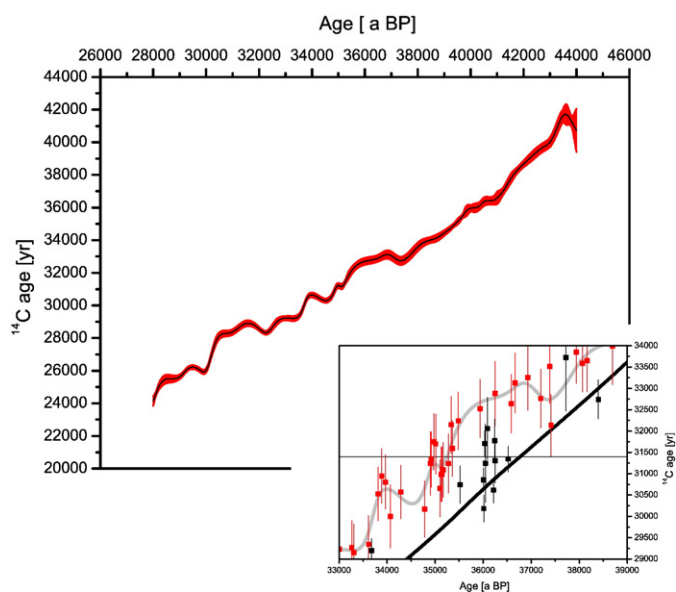


Fig. 9. Terrestrial ^{14}C age comparison curve for the time 44–28 ka BP based on speleothem GB89-25-3. The curve is derived by a smoothing cubic spline, the $1\text{-}\sigma$ confidence band is indicated in red. The inset shows the GB89-25-3 ^{14}C age data (red symbols) and the speleothem comparison curve spline (grey line) between 29 and 34 kyr ^{14}C age together with ^{14}C age data and calibration curve of Fairbanks et al. (2005) (black symbols and line). The thin horizontal line indicates the ^{14}C age of a charcoal drawing in Chauvet cave (31.4 kyr) and highlights the implications for the comparison calendar ages due to differences between the terrestrial and marine data set.

Charcoal drawings in the Chauvet cave, for example, with an uncalibrated ^{14}C age of 31.4 ± 0.6 kyr (Bard et al., 2004b; Valladas et al., 2001), yield calendar ages of around 35.3 ka based on our new speleothem comparison curve and 36.8 ka based on the Fairbanks calibration curve as shown in Fig. 9. The apparent age difference due to the chosen calibration curve renders many results equivocal. This is particularly true where, for example, the timing of modern human and Neanderthal occupation is compared with records of climate change during the last glacial period, when temperatures fluctuated dramatically at millennial timescales (Gravina et al., 2005). A difference of ~ 1 ka for level B1-3 at Chatelperron (Gravina et al., 2005) with 40–41 ka and 39–40 ka using a marine and our terrestrial comparison curve, respectively, leaves the interpretation that B1-3 was deposited during a warm spell during the last glacial (Gravina et al., 2005) in some doubt. This highlights the intense need for an accurate and coherent community-accepted calibration. Hopefully, our current contribution from the terrestrial realm provides a move in that direction.

Acknowledgement

This research was supported by the NERC (NER/A/S/2001/00526), the Leverhulme Trust (F/00 182/AU) and the NSF (EAR0223311, EAR0446861 and EAR0622305). We thank J.S. Pigati and J. Quade for use of their new low-blank ^{14}C preparation line. We also acknowledge C. Coath for technical assistance at BIG facilities and J. Tooby for preparing one of the figures. Andy Ridgwell is acknowledged for help with the GENIE model.

Appendix A. Supplementary data

Supplementary data associated with this article can be found in the online version at doi:10.1016/j.epsl.2009.10.004.

References

- Anikovitch, M.V., Sinitsyn, A.A., Hoffecker, J.F., Holliday, V.T., Popov, V.V., Lisitsyn, S.N., Forman, S.L., Levkovskaya, G.M., Pospelova, G.A., Kuz'mina, I.E., Burova, N.D., Goldberg, P., Macphail, R.I., Giaccio, B., Praslov, N.D., 2007. Early Upper Paleolithic in Eastern Europe and implications for the dispersal of modern humans. *Science* 315, 223–226.
- Bard, E., 1998. Geochemical and geophysical implications of the radiocarbon calibration. *Geochim. Cosmochim. Acta* 62, 2025–2038.
- Bard, E., Hamelin, B., Fairbanks, R.G., Zindler, A., 1990. Calibration of the C-14 timescale over the past 30,000 years using mass-spectrometric U-Th ages from Barbados Corals. *Nature* 345, 405–410.
- Bard, E., Menot-Combes, G., Rostek, F., 2004a. Present status of radiocarbon calibration and comparison records based on Polynesian corals and Iberian Margin sediments. *Radiocarbon* 46, 1189–1202.
- Bard, E., Rostek, F., Menot-Combes, G., 2004b. A better radiocarbon clock. *Science* 303, 178–179.
- Bard, E., Rostek, F., Menot-Combes, G., 2004c. Radiocarbon calibration beyond 20,000 C-14 yr BP by means of planktonic foraminifera of the Iberian Margin. *Quatern. Res.* 61, 204–214.
- Beck, J.W., Richards, D.A., Edwards, R.L., Silverman, B.W., Smart, P.L., Donahue, D.J., Hererra-Osterheld, S., Burr, G.S., Calsoyas, L., Jull, A.J.T., Biddulph, D., 2001. Extremely large variations of atmospheric C-14 concentration during the last glacial period. *Science* 292, 2453–2458.
- Broecker, W.S., 1963. Radioisotopes and large scale oceanic mixing. In: Hill, M.N. (Ed.), *The Sea*. Interscience Publishers, New York, pp. 88–108.
- Burr, G.S., Edwards, R.L., Donahue, D.J., Druffel, E.R.M., Taylor, F.W., 1992. Mass-spectrometric C-14 and U-Th measurements in coral. *Radiocarbon* 34, 611–618.
- Burr, G.S., Galang, C., Taylor, F.W., Gallup, C., Edwards, R.L., Cutler, K., Quirk, B., 2004. Radiocarbon results from a 13-kyr BP coral from the Huon Peninsula, Papua New Guinea. *Radiocarbon* 46, 1211–1224.
- Burr, G.S., Donahue, D.J., Tang, Y., Beck, J.W., McHargue, L., Biddulph, D., Cruz, R., Jull, A.J.T., 2007. Error analysis at the NSF-Arizona AMS facility. *Nucl. Instrum. Methods Phys. Res., B Beam Interact. Mater. Atoms* 259, 149–153.
- Carcaillet, J., Bourles, D.L., Thouveny, N., Arnold, M., 2004. A high resolution authigenic Be-10/Be-9 record of geomagnetic moment variations over the last 300 ka from sedimentary cores of the Portuguese margin. *Earth Planet. Sci. Lett.* 219, 397–412.
- Cheng, H., Edwards, R.L., Hoff, J., Gallup, C.D., Richards, D.A., Asmerom, Y., 2000. The half-lives of uranium-234 and thorium-230. *Chem. Geol.* 169, 17–33.
- Cutler, K.B., Gray, S.C., Burr, G.S., Edwards, R.L., Taylor, F.W., Cabioch, G., Beck, J.W., Cheng, H., Moore, J., 2004. Radiocarbon calibration and comparison to 50 kyr BP with paired C-14 and Th-230 dating of corals from Vanuatu and Papua New Guinea. *Radiocarbon* 46, 1127–1160.
- Elsasser, W., Ney, E.P., Winckler, J.R., 1956. Cosmic-ray intensity and geomagnetism. *Nature* 178, 1226–1227.
- Fairbanks, R.G., Mortlock, R.A., Chiu, T.C., Cao, L., Kaplan, A., Guilderson, T.P., Fairbanks, T.W., Ales, A.L., Grootes, P.M., Nadeau, M.J., 2005. Radiocarbon calibration curve spanning 0 to 50,000 years BP based on paired Th-230/U-234/U-238 and C-14 dates on pristine corals. *Quatern. Sci. Rev.* 24, 1781–1796.
- Friedrich, M., Remmele, S., Kromer, B., Hofmann, J., Spurk, M., Kaiser, K.F., Orzel, C., Kuppers, M., 2004. The 12,460-year Hohenheim oak and pine tree-ring chronology from central Europe – A unique annual record for radiocarbon calibration and paleoenvironment reconstructions. *Radiocarbon* 46, 1111–1122.
- Genty, D., Massault, M., Gilmour, M., Baker, A., Verheyden, S., Kepens, E., 1999. Calculation of past dead carbon proportion and variability by the comparison of AMS(^{14}C) and TIMS U/Th ages on two holocene stalagmites. *Radiocarbon* 41, 251–270.
- Gravina, B., Mellars, P., Ramsey, C.B., 2005. Radiocarbon dating of interstratified Neanderthal and early modern human occupations at the Chatelperronian type-site. *Nature* 438, 51–56.
- Guillou, H., Singer, B.S., Laj, C., Kissel, C., Scaillet, S., Jicha, B.R., 2004. On the age of the Laschamp geomagnetic excursion. *Earth Planet. Sci. Lett.* 227, 331–343.
- Hoffmann, D.L., Prytulak, J., Richards, D.A., Elliott, T., Coath, C.D., Smart, P.L., Scholz, D., 2007. Procedures for accurate U and Th isotope measurements by high precision MC-ICPMS. *Int. J. Mass Spectrom.* 264, 97–109.
- Holden, N.E., 1990. Total half-lives for selected nuclides. *Pure Appl. Chem.* 62, 941–958.
- Hughen, K.A., Overpeck, J.T., Lehman, S.J., Kashgarian, M., Southon, J., Peterson, L.C., Alley, R., Sigman, D.M., 1998. Deglacial changes in ocean circulation from an extended radiocarbon calibration. *Nature* 391, 65–68.
- Hughen, K., Lehman, S., Southon, J., Overpeck, J., Marchal, O., Herring, C., Turnbull, J., 2004. C-14 activity and global carbon cycle changes over the past 50,000 years. *Science* 303, 202–207.
- Hughen, K., Southon, J., Lehman, S., Bertrand, C., Turnbull, J., 2006. Marine-derived C-14 calibration and activity record for the past 50,000 years updated from the Cariaco Basin. *Quatern. Sci. Rev.* 25, 3216–3227.
- Jackson, A.S., McDermott, F., Mangini, A., 2008. Late Holocene climate oscillations and solar fluctuations from speleothem STAL-AH-1, Sauerland, Germany: A numerical perspective. *Geophys. Res. Lett.* 35, L06702.
- Jaffey, A.H., Flynn, K.F., Glendenin, L.E., Bentley, W.C., Essling, A.M., 1971. Precision measurement of half-lives and specific activities of U-235 and U-238. *Phys. Rev. C* 4, 1889–1906.
- Jouzel, J., Masson-Delmotte, V., Cattani, O., Dreyfus, G., Falourd, S., Hoffmann, G., Minster, B., Nouet, J., Barnola, J.M., Chappellaz, J., Fischer, H., Gallet, J.C., Johnsen, S., Leuenberger, M., Loulergue, L., Luethi, D., Oerter, H., Parrenin, F., Raisbeck, G., Raynaud, D., Schilt, A., Schwander, J., Selmo, E., Souchez, R., Spahni, R., Stauffer, B., Steffensen, J.P., Stenni, B., Stocker, T.F., Tison, J.L., Werner, M., Wolff, E.W., 2007.

- Orbital and millennial Antarctic climate variability over the past 800,000 years. *Science* 317, 793–796.
- Laj, C., Kissel, C., Beer, J., 2004. High resolution global paleointensity stack since 75 kyr (GLOPIS-75) calibrated to absolute values. *Timescales of the Paleomagnetic Field* 145, 255–265.
- Lal, D., Peters, B., 1967. Cosmic ray produced radioactivity on the Earth. In: Flüggé, S. (Ed.), *Handbuch für Physik*. Springer, Berlin, pp. 551–612.
- Leduc, G., Thouveny, N., Bourles, D.L., Blanchet, C.L., Carcaillet, J.T., 2006. Authigenic Be-10/Be-9 signature of the Laschamp excursion: a tool for global synchronisation of paleoclimatic archives. *Earth Planet. Sci. Lett.* 245, 19–28.
- Lenton, T.M., Williamson, M.S., Edwards, N.R., Marsh, R., Price, A.R., Ridgwell, A.J., Shepherd, J.G., Cox, S.J., 2006. Millennial timescale carbon cycle and climate change in an efficient Earth system model. *Climate Dynamics* 26, 687–711.
- Marsh, R., Smith, M.P.L.M., Rohling, E.J., Lunt, D.J., Lenton, T.M., Williamson, M.S., Yool, A., 2006. Modelling ocean circulation, climate and oxygen isotopes in the ocean over the last 120 000 years. *Clim. Past Discuss.* 2, 657–709.
- Masarik, J., Beer, J., 1999. Simulation of particle fluxes and cosmogenic nuclide production in the Earth's atmosphere. *J. Geophys. Res.-Atmos.* 104, 12099–12111.
- Matsumoto, K., Sarmiento, J.L., Key, R.M., Aumont, O., Bullister, J.L., Caldeira, K., Campin, J.M., Doney, S.C., Drange, H., Dutay, J.C., Follows, M., Gao, Y., Gnanadesikan, A., Gruber, N., Ishida, A., Joos, F., Lindsay, K., Maier-Reimer, E., Marshall, J.C., Matear, R.J., Monfray, P., Mouchet, A., Najjar, R., Plattner, G.K., Schlitzer, R., Slater, R., Swathi, P.S., Totterdell, I.J., Weirig, M.F., Yamanaka, Y., Yool, A., Orr, J.C., 2004. Evaluation of ocean carbon cycle models with data-based metrics. *Geophys. Res. Lett.* 31, L07303.
- Meese, D.A., Gow, A.J., Alley, R.B., Zielinski, G.A., Grootes, P.M., Ram, M., Taylor, K.C., Mayewski, P.A., Bolzan, J.F., 1997. The Greenland Ice Sheet Project 2 depth-age scale: methods and results. *J. Geophys. Res.-Oceans* 102, 26411–26423.
- Meissner, K.J., Schmittner, A., Weaver, A.J., Adkins, J.F., 2003. Ventilation of the North Atlantic Ocean during the Last Glacial Maximum: A comparison between simulated and observed radiocarbon ages. *Paleoceanography* 18, 1023.
- Mellars, P., 2006. A new radiocarbon revolution and the dispersal of modern humans in Eurasia. *Nature* 439, 931–935.
- Muscheler, R., Beer, R., Kubik, P.W., Synal, H.A., 2005. Geomagnetic field intensity during the last 60, 000 years based on Be-10 and Cl-36 from the Summit ice cores and C-14. *Quatern. Sci. Rev.* 24, 1849–1860.
- Muscheler, R., Kromer, B., Björck, S., Svensson, A., Friedrich, M., Kaiser, K.F., Southon, J., 2008. Tree rings and ice cores reveal C-14 calibration uncertainties during the Younger Dryas. *Nat. Geosci.* 1, 263–267.
- Petit, J.R., Jouzel, J., Raynaud, D., Barkov, N.I., Barnola, J.M., Basile, I., Bender, M., Chappellaz, J., Davis, M., Delaygue, G., Delmotte, M., Kotlyakov, V.M., Legrand, M., Lipenkov, V.Y., Lorius, C., Pepin, L., Ritz, C., Saltzman, E., Stevenard, M., 1999. Climate and atmospheric history of the past 420,000 years from the Vostok ice core, Antarctica. *Nature* 399, 429–436.
- Pigati, J.S., Quade, J., Wilson, J., Jull, A.J.T., Lifton, N.A., 2007. Development of low-background vacuum extraction and graphitization systems for C-14 dating of old (40–60 ka) samples. *Quatern. Int.* 166, 4–14.
- Price, A.R., Voutchkov, I.I., Pound, G.E., Edwards, N.R., Lenton, T.M., Cox, S.J., 2006. Multiobjective tuning of grid-enabled earth system models using a non-dominated sorting genetic algorithm (NSGA-II). *Second IEEE International Conference on e-Science and Grid Computing*, Amsterdam, p. 117.
- Reimer, P.J., Baillie, M.G.L., Bard, E., Bayliss, A., Beck, J.W., Bertrand, C.J.H., Blackwell, P.G., Buck, C.E., Burr, G.S., Cutler, K.B., Damon, P.E., Edwards, R.L., Fairbanks, R.G., Friedrich, M., Guilderson, T.P., Hogg, A.G., Hughen, K.A., Kromer, B., McCormac, G., Manning, S., Ramsey, C.B., Reimer, R.W., Remmele, S., Southon, J.R., Stuiver, M., Talamo, S., Taylor, F.W., van der Plicht, J., Weyhenmeyer, C.E., 2004. IntCal04 terrestrial radiocarbon age calibration, 0–26 cal kyr BP. *Radiocarbon* 46, 1029–1058.
- Reimer, P.J., Baillie, M.G.L., McCormac, G., Reimer, R.W., Bard, E., Beck, J.W., Blackwell, P.G., Buck, C.E., Burr, G.S., Edwards, R.L., Friedrich, M., Guilderson, T.P., Manning, S., Guilderson, T.P., Southon, J.R., Hogg, A.G., Stuiver, M., Hughen, K.A., van der Plicht, J., Kromer, B., van der Plicht, J., Manning, S., Weyhenmeyer, C.E., 2006. Comment on “Radiocarbon calibration curve spanning 0 to 50,000 years BP based on paired Th-230/U-234/U-238 and C-14 dates on pristine corals” by R.G. Fairbanks et al. (*Quaternary Science Reviews* 24 (2005) 1781–1796) and “Extending the radiocarbon calibration beyond 26,000 years before present using fossil corals” by T.-C. Chin et al. (*Quaternary Science Reviews* 24 (2005) 1797–1808). *Quat. Sci. Rev.* 25, 855–862.
- Ridgwell, A., Hargreaves, J.C., Edwards, N.R., Annan, J.D., Lenton, T.M., Marsh, R., Yool, A., Watson, A., 2007. Marine geochemical data assimilation in an efficient Earth System Model of global biogeochemical cycling. *Biogeosciences* 4, 87–104.
- Sarnthein, M., Grootes, P.M., Kennett, J.P., Nadeau, M.-J., 2007. 14C reservoir ages show deglacial changes in ocean currents and carbon cycle. In: Schmittner, A., Chiang, J., Hemmings, S. (Eds.), *Ocean Circulation: Mechanisms and Impacts*. : Geophysical Monograph Series. AGU, pp. 175–196.
- Shackleton, N.J., Fairbanks, R.G., Chiu, T.C., Parrenin, F., 2004. Absolute calibration of the Greenland time scale: implications for Antarctic time scales and for Delta C-14. *Quatern. Sci. Rev.* 23, 1513–1522.
- Singarayer, J.S., Richards, D.A., Ridgwell, A., Valdes, P.J., Austin, W.E.N., Beck, J.W., 2008. An oceanic origin for the increase of atmospheric radiocarbon during the Younger Dryas. *Geophys. Res. Lett.* 35, L14707.
- Stuiver, M., 1982. A high-precision calibration of the ad radiocarbon time scale. *Radiocarbon* 24, 1–26.
- Stuiver, M., Braziunas, T.F., 1993. Modeling atmospheric C-14 influences and C-14 ages of marine samples to 10,000 Bc. *Radiocarbon* 35, 137–189.
- Stuiver, M., Reimer, P.J., Bard, E., Beck, J.W., Burr, G.S., Hughen, K.A., Kromer, B., McCormac, G., Van der Plicht, J., Spurk, M., 1998. IntCal98 radiocarbon age calibration, 24, 000–0 cal BP. *Radiocarbon* 40, 1041–1083.
- Svensson, A., Andersen, K.K., Bigler, M., Clausen, H.B., Dahl-Jensen, D., Davies, S.M., Johnsen, S.J., Muscheler, R., Parrenin, F., Rasmussen, S.O., Roethlisberger, R., Seierstad, I., Steffensen, J.P., Vinther, B.M., 2008. A 60 000 year Greenland stratigraphic ice core chronology. *Clim. Past* 4, 47–57.
- Toggweiler, J.R., Dixon, K., Bryan, K., 1989. Simulations of radiocarbon in a coarse-resolution world ocean model. 1. Steady-State prebomb distributions. *J. Geophys. Res.-Oceans* 94, 8217–8242.
- Trenberth, K., Olson, J., Large, W., 1989. Tech. Rep. NCAR/TN-338+STR. National Center for Atmospheric Research, Boulder, Colorado.
- Valladas, H., Clottes, J., Geneste, J.M., Garcia, M.A., Arnold, M., Cachier, H., Tisnerat-Laborde, N., 2001. Palaeolithic paintings – evolution of prehistoric cave art. *Nature* 413, 479.
- van der Plicht, J., Beck, J.W., Bard, E., Baillie, M.G.L., Blackwell, P.G., Buck, C.E., Friedrich, M., Guilderson, T.P., Hughen, K.A., Kromer, B., McCormac, G., Ramsey, C.B., Reimer, P.J., Reimer, R.W., Remmele, S., Richards, D.A., Southon, J.R., Stuiver, M., Weyhenmeyer, C.E., 2004. NotCal04 – comparison/calibration C-14 records 26–50 cal kyr BP. *Radiocarbon* 46, 1225–1238.
- Voelker, A.H.L., Sarnthein, M., Grootes, P.M., Erlenkeuser, H., Laj, C., Mazaud, A., Nadeau, M.J., Schleicher, M., 1998. Correlation of marine C-14 ages from the Nordic Seas with the GISP2 isotope record: implications for C-14 calibration beyond 25 ka BP. *Radiocarbon* 40, 517–534.
- Vogel, J.C., 1983. C-14 variations during the Upper Pleistocene. *Radiocarbon* 25, 213–218.
- Vogel, J.C., Kronfeld, J., 1997. Calibration of radiocarbon dates for the late Pleistocene using U/Th dates on stalagmites. *Radiocarbon* 39, 27–32.
- Wang, Y.J., Cheng, H., Edwards, R.L., An, Z.S., Wu, J.Y., Shen, C.C., Dorale, J.A., 2001. A high-resolution absolute-dated Late Pleistocene monsoon record from Hulu Cave, China. *Science* 294, 2345–2348.
- Wang, X.F., Auler, A.S., Edwards, R.L., Cheng, H., Ito, E., Solheid, M., 2006. Interhemispheric anti-phasing of rainfall during the last glacial period. *Quatern. Sci. Rev.* 25, 3391–3403.
- Wedepohl, K.H., 1995. The composition of the continental-crust. *Geochim. Cosmochim. Acta* 59, 1217–1232.
- Weninger, B., Joris, O., 2008. A C-14 age calibration curve for the last 60 ka: the Greenland-Hulu U/Th timescale and its impact on understanding the Middle to Upper Paleolithic transition in Western Eurasia. *J. Hum. Evol.* 55, 772–781.
- Williamson, M.S., Lenton, T.M., Shepherd, J.G., Edwards, N.R., 2006. An efficient numerical terrestrial scheme (ENTS) for Earth system modelling. *Ecol. Model.* 198, 362–374.